Journal of Alloys and Compounds, 211/212 (1994) 296–299
JALCOM 087

Oxygen mobility in $YBa_2Cu_3O_{7-\delta}$

P. Gadaud
LMPM, ENSMA, Rue Guillaume VII, F-86034 Poitiers (France)

B. Kaya
LMP, Université de Poitiers, Poitiers (France)

Abstract

The aim of this experimental study is to characterize the oxygen mobility in CuO confined planes in the high T_c superconductor YBaCuO by means of a very low frequency mechanical spectroscopy technique allowing measurements in a temperature range where the oxygen concentration remains stable.

For oxygen-rich specimens corresponding to the orthorhombic I phase we observe a single relaxation peak. The measured activation energy E_I varies between 0.8 and 1.3 eV and is a complex function of the oxygen concentration. For less rich oxygen contents a second relaxation peak is observed coexisting with the first peak. Its energy E_{TII} is about 1.10 eV, independent of the concentration. A model of oxygen jumps in CuO planes is proposed to explain these results.

1. Introduction

The large scattering of oxygen relaxation parameters in CuO planes in the high T_c superconductor YBaCuO reported by various authors [1–7] indicates that the oxygen concentration, correlated with the degree of anisotropy in these planes, is the most important factor influencing the apparent relaxation characteristics. Several models [5, 8, 9] take into account the anisotropy to explain some modifications in oxygen jump rates.

We propose here to describe the oxygen mobility as a function of its concentration, using a very low frequency mechanical spectroscopy technique. This allows an isothermal characterization of a mechanism apparently dependent on the oxygen population at thermodynamical equilibrium.

2. Experimental details

The specimens were fabricated in the Laboratoire de Métallurgie Physique from Y_2O_3, CuO and Ba CO_2 powders. The melt was calcined twice at 1223 K for 6 and 12 h, finely ground under an isostatic pressure of 3800 bar, then flat bars were machined and sintered in air for 40 h at 1223 K.

Various phases of reoxygenation have been realized to obtain different amounts of oxygen: 3 h at 723 K, 5 h at 833 K with and without an oxygen flow, 2 h at 720 K in the atmosphere. The specimens have been characterized by X-ray and chemical analysis to determine the oxygen concentration precisely. They all showed a marked Meissner effect.

Experimental specimens ($25 \times 4 \times 1.5$ mm^3) were fixed into the apparatus grips by a system of foils and pins [10], allowing us to clamp very brittle specimens.

Measurements were performed by frequency sweeping under high vacuum. Between successive measurements samples were annealed *in situ* at higher temperatures to reduce the oxygen content. All the thermal treatments have been reproduced in another furnace under the same conditions and the new oxygen concentrations analysed. It was possible to obtain several oxygen mobility characterizations from one given specimen.

3. Experimental results

Damping effects have been observed in the temperature range 400–500 K. Because of their reproducibility, we assume that there is no oxygen loss during the measurements under vacuum in this temperature range.

The typical evolution of the damping spectrum with successive annealings is shown in Fig. 1. We can see that from the initial relaxation peak P_I (related to higher oxygen concentrations) a second peak P_{TII} develops after higher temperature annealings (lower concentrations) as observed by other authors [11, 12].

SSDI 0925-8388(93)00087-F

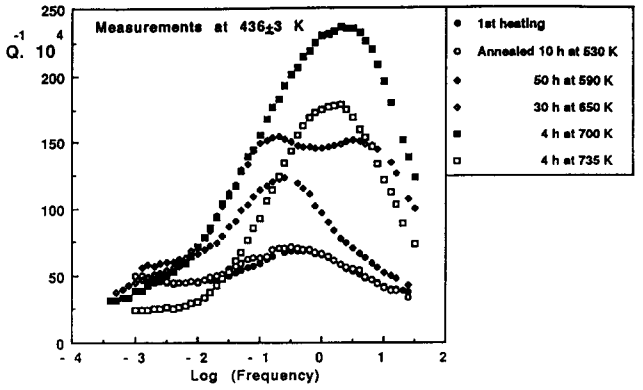

Fig. 1. Evolution of isothermal damping with successive annealings (measurements at 436±3 K). The reference specimen contained $1-\delta=0.817$ oxygen in CuO planes.

As an example, Fig. 2(a) shows the measured damping spectra after annealing at 700 K, Fig. 2(b) the corresponding dynamical modulus evolution, Fig. 2(c) the decomposition of a damping spectrum into two symmetric relaxation peaks (frequency sweep at 438 K) and Fig. 2(d) the deduced Arrhenius laws for the two relaxation peaks.

This decomposition allows us to determine the strength of the two relaxations. These strengths are reported as a function of the oxygen concentration in Fig. 3 (specimen analysis after thermal treatments).

Peak P_{TII} is only present for lower oxygen concentrations corresponding to the orthorhombic II phase; in contrast, peak P_I exists for all concentrations.

3.1. P_I peak

The measured activation energy E_I and limit time constant τ_{oI} are given in Table 1 for various oxygen concentrations. Figure 4 shows the complex evolution of the activation energy. In particular, we can observe the fast decrease in the apparent energy for concentrations corresponding to the orthorhombic I phase, thus explaining the large scattering observed in the literature.

3.2. P_{TII} peak

This relaxation peak, related to the orthorhombic II phase, is associated with very stable dynamical parameters as seen in Table 2. This indicates that the responsible mechanism could be associated with a Snoek-type relaxation.

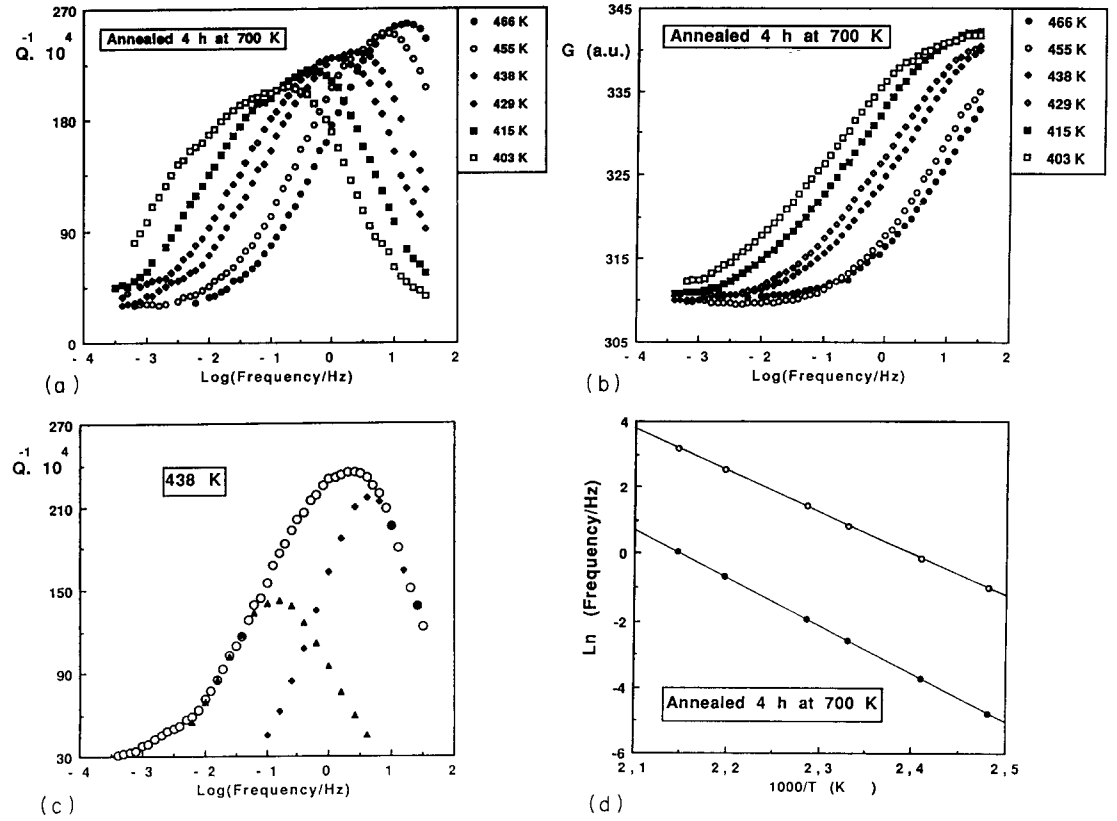

Fig. 2. (a) Damping curves obtained after annealing at 700 K. (b) Dynamical modulus curves corresponding to (a). (c) Decomposition of damping spectrum into two symmetric relaxation peaks (measurements at 438 K). (d) Deduced Arrhenius laws for the two peaks in (c): ●, P_I, $E_I=1.25$ eV, $\tau_{oI}=4\times10^{-15}$ s; ○, P_{TII}, $E_{II}=1.09$ eV, $\tau_{oTII}=1.5\times10^{-14}$ s.

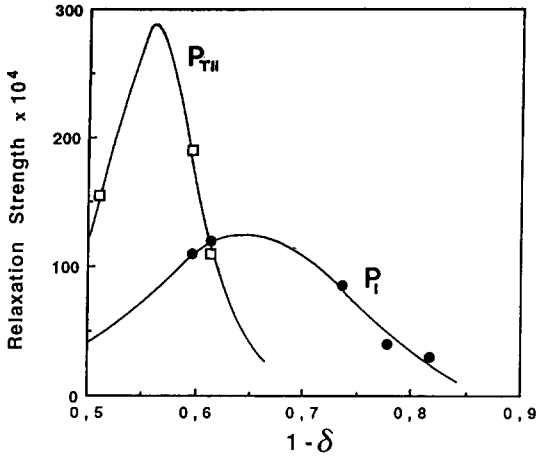

Fig. 3. Evolution of relaxation strengths as a function of oxygen concentration (relaxation peak amplitude taken at 433 K).

TABLE 1. Characteristics of peak P_I

Oxygen concentration $(1-\delta)$	E_I (eV)	τ_{oI} (s)	$-\log \tau_{oI}/E_I$
0.817	1.15	2×10^{-14}	27.43
0.807	1.07	2.4×10^{-13}	27.16
0.806	1.02	9×10^{-13}	27.19
0.778	0.87	4.6×10^{-11}	27.36
0.736	0.89	3×10^{-11}	27.22
0.650	1.23	3.4×10^{-15}	27.08
0.614	1.32	9×10^{-16}	26.25
0.596	1.25	4×10^{-15}	26.52

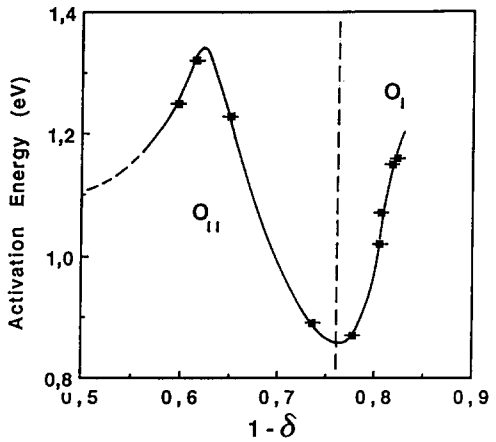

Fig. 4. Evolution of activation energy of peak P_I as a function of oxygen concentration.

4. Discussion

Classically, an energy gap ΔE is defined between the two types of sites along the a and b axes for oxygen atoms in CuO planes. The anisotropy is then represented by the difference between the populations C_A and C_B ($C_A+C_B=1-\delta=C_o$) along the respective axes.

TABLE 2. Characteristics of peak P_{TII}

Oxygen concentration $(1-\delta)$	E_{TII} (eV)	τ_{oTII} (10^{14} s)
0.665	1.08	1.4
0.614	1.13	1.2
0.596	1.09	1.4
0.510	1.08	1.5

The total jump rate between neighbouring sites is expressed by

$$\nu=4\nu_D\left[C_A(1-C_B)\exp\left(-\frac{E}{kT}\right)-C_B(1-C_A)\exp\left(-\frac{\Delta E+E}{kT}\right)\right] \quad (1)$$

where ν_D is the Debye frequency, E is the site energy level in the isotropic tetragonal phase and $1-C_B$ and $1-C_A$ are the respective probabilities for neighbouring sites to be free.

The thermodynamical equilibrium is described by the relation

$$C_A(1-C_B)=C_B(1-C_A)\exp\left(-\frac{\Delta E}{kT}\right) \quad (2)$$

This relation is different from Boltzmann's law, which is only valid for dilute populations.

If we adopt the model proposed by Mi *et al.* [8] and introduce this new condition of thermodynamical equilibrium, we can obtain an expression for the relaxation time depending on both temperature and concentration:

$$\tau_o(T, C_o)=\frac{1}{\nu_D}\exp\left(\frac{E}{kT}\right)\frac{1+\tanh\left(\frac{\Delta E}{2kT}\right)}{\left[1-C_o(2-C_o)\tanh^2\left(\frac{\Delta E}{2kT}\right)\right]^{1/2}} \quad (3)$$

To explain the existence of two relaxation peaks in the orthorhombic II phase, we consider that the lattice can be divided in two sublattices (Fig. 5); we obtain a first relaxation between equivalent sites as could be described in the tetragonal phase (Snoek-type relaxation) and a second relaxation corresponding to that proposed in the orthorhombic I phase. However, if we take into account the population distribution in the orthorhombic II phase, we obtain a new condition of thermodynamical equilibrium:

$$|2C_B-C_A||1-C_A|\exp\left(\frac{\Delta E}{kT}\right)=C_A|1-2C_B+C_A| \quad (4)$$

The complete calculation will be given elsewhere.

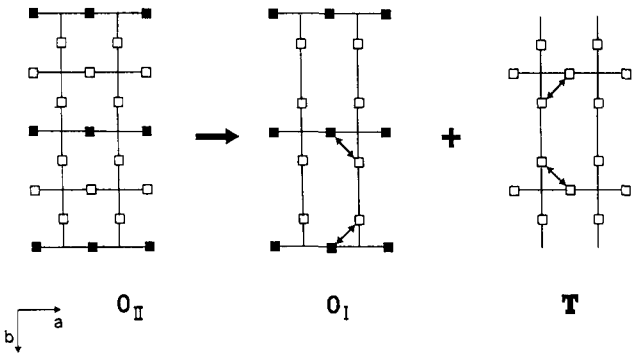

Fig. 5. The two relaxations in the orthorhombic II phase: between equivalent sites (□) and between different energy level sites.

This approach can explain that the observed relaxation time is a function of both temperature and concentration and that the orthorhombic I–II transition has an influence on the thermodynamical equilibrium and thus on the evolution of the relaxation time. This description is based on the jump probability between random populations of atoms along the *a* and *b* axes. The next development of this model will be to take into account the long-range order along the *b* axis, which certainly affects the local jump probabilities.

References

1 B.S. Berry, *Bull. Am. Phys. Soc., 33* (1988) 512.
2 J.L. Tallon, A.K. Schuitema and N.E. Tapp, *Appl. Phys. Lett., 52* (1988) 507.
3 J.X. Zhang, G.R. Lin, Z.C. Lin, K.F. Liang, P.C.W. Fung and G.G. Siu, *J. Phys.: Condens. Matter, 1* (1989) 6939.
4 X.M. Xie, T.G. Chen and Z.L. Wu, *Phys. Rev. B, 40* (1989) 4549.
5 J.R. Cost and J.T. Stanley, *J. Mater. Res., 6* (1991) 232.
6 J. Woirgard, A. Riviere, P. Gadaud and P. Tal, *Europhys. Lett., 17* (1992) 601.
7 Y. Mi, D. Mari, R. Schaller and W. Benoit, *Mater. Sci. Forum, 119–121* (1993) 707.
8 Y. Mi, T. Schaller, S. Sathish and W. Benoit, *Phys. Rev. B, 44* (1991) 12575.
9 X.M. Xie, T.G. Chen and H. Huang, *Phys. Status Solidi A, 110* (1988) 415.
10 J. Woirgard, Ph. Mazot and A. Riviere, *J. Phys. (Paris), 10* (1981) 1135.
11 E. Bonetti, E.G. Campari, T. Manfredini and S. Mantovani, *Physica C, 196* (1991) 17.
12 G. Cannelli, R. Cantelli, F. Cordero and F. Trequattrini, *Supercond. Sci. Technol., 5* (1992) 247.